Materials Science & Engineering A 849 (2022) 143502

Contents lists available at ScienceDirect

Materials Science & Engineering A

journal homepage: www.elsevier.com/locate/msea

Investigation of novel post-thermal treatments of alloy 718 fabricated by modulated laser powder bed fusion

Konstantinos Georgilas [a,b,c], Alessandro Sergi [b,c], Raja H.U. Khan [c], Mehmet E. Kartal [a,*]

[a] University of Aberdeen, School of Engineering, Aberdeen, AB24 3UE, UK
[b] National Structural Integrity Research Centre, Cambridge, CB21 6AL, UK
[c] TWI Ltd., Cambridge, CB21 6AL, UK

ARTICLE INFO

Keywords:
Electron microscopy
Characterisation
Nickel alloys
Laser methods
Powder methods

ABSTRACT

The aim of this work is to determine the impact of post-thermal treatments on the mechanical properties and microstructure of alloy 718 superalloy manufactured through modulated laser powder bed fusion. Three post-thermal treatments at 980 °C and 1200 °C with and without hot isostatic pressing are utilised, followed by standard ageing procedure. The tensile mechanical properties, microstructure, crystallography, morphology, fracture impact and hardness after each heat treatment are determined. It has been found that the heat treatment procedure at 980 °C significantly affects the tensile properties while leading to no change in grain size or orientation, and formation of twined grains. A temperature of 1200 °C with and without pressure causes considerable grain growth in comparison with the as-built and 980 conditions and significant formation of twinned grains. Hot isostatic pressing was found to produce the tensile mechanical properties close to those of wrought alloy 718.

1. Introduction

Alloy 718 is a precipitation strengthened Ni-base superalloy. It is mainly strengthened by the precipitation of the metastable gamma double prime (γ'') [Ni_3Nb] hardening phase, that precipitates as consequence of the aging heat treatment [1]. Thus, post-thermal treatment is required to achieve the final mechanical properties of alloy 718 material regardless of manufacturing methods used. Considerable knowledge and standards exist on heat treating (HT) alloy 718, produced through traditional manufacturing methods. Existing HT standards have been extensively applied to Additive Manufacturing (AM) materials with varying results [2–4]. Current HT standards applied to AM material, lead to improvement in the mechanical properties over the as-built condition. However, heat treatment results are not consistent between research works and quite commonly do not satisfy the minimum required properties as defined by the same standards [2]. In addition, these standards are not adequate to drastically reduce anisotropy of the crystal microstructure between the Z and XY directions in as-built alloy 718. Thus, as consequence of the anisotropy, the mechanical properties are strongly dependent on the loading direction.

Limited investigations have been performed on the heat treatment of alloy 718 above 1100 °C [5–9], where a variety of cooling methods and holding times have been assessed. However, these studies have not generally been systematic repeating the same or very similar heat treatment regimens. Post-thermal treatment by hot isostatic pressing (HIP) can represent a valid solution to achieve the desired strength for alloy 718, however even fewer investigations concerning this post-thermal treatment have been performed [10–12]. Treatments at higher temperatures show promise in regard to decreasing microstructural anisotropy by way of recrystallization and grain growth. The decrease in anisotropy also results in more isotropic mechanical properties and thus more predictable material response.

Regarding alloy 718 material produced through modulated laser powder bed fusion (L-PBF) no work on HT has been carried out. Modulated L-PBF material shows similarities to continuous L-PBF material regarding phase composition, such as the extensive propagation of Laves phase as demonstrated in the previous study [13]. However, the crystal microstructure was shown to be completely different in the Z direction with weaker texture present [13]. Hence, there is a gap in the state-of-the-art regarding the response of modulated L-PBF alloy 718 material to heat treatment.

This paper will present the results of heat treatments performed on alloy 718 specimens manufactured using the modulated L-PBF process. Three separate post-thermal treatments were performed. First at 980 °C

* Corresponding author.
E-mail address: mehmet.kartal@abdn.ac.uk (M.E. Kartal).

https://doi.org/10.1016/j.msea.2022.143502
Received 11 March 2022; Received in revised form 19 June 2022; Accepted 22 June 2022
Available online 24 June 2022

according to AMS5663N [16], which will be called 980. Second, a novel solution heat treatment at 1200 °C, called SHT. Third, hot isostatic pressing (HIP) at 1200 °C, called HIP.

2. Material and methods

Gas atomised alloy 718 metal powder (supplied by LPW technology, Widnes, UK) with a size range of 15–45 μm was used for manufacturing all the specimens by using the modulated laser PBF process. Samples were manufactured using an AM250 machine built by Renishaw (Gloucestershire, UK). The laser power used was 200W and the exposure time was 110 μm. The reasoning behind the parameters used in manufacturing is due to produced parts with the highest densification, as was investigated elsewhere [13]. Specimens manufactured include cubes, tensile blanks and Charpy blanks.

Specimens were subjected to three different heat treatment profiles, followed by aging treatment. The heat treatment parameters are summarised in Table 1 below. The 980, SHT and aging heat treatments were performed in a vacuum furnace located at TWI Ltd. The furnace can achieve vacuum levels of 10^{-6} MPa at a maximum temperature of 1200 °C and is equipped with argon fast cool capabilities. HIP treatment was performed in a HIP vessel at the University of Birmingham. The vessel can withstand 200 MPa and 1450 °C and is equipped with argon fast cool. For all post-thermal treatments, temperature was controlled and monitored using Type K thermocouples.

Cube specimens in both the as-built and heat-treated conditions were metallographically prepared using silicon carbide (SiC) grinding papers of different grits and suspension solutions. Greater details about the metallographic preparation and specimen characterisation have been provided in the previous work of the authors [13]. Specimens were characterised using optical microscopy to measure material density by image analysis using ImageJ software. Specimens were also subjected to scanning electron microscopy (SEM) and electron backscatter diffraction (EBSD) to determine the crystal microstructure. The polished cube specimens were also hardness tested using a micro Vickers hardness tester.

The tensile blanks were manufactured in three different build directions: vertical, horizontal and 45°. The vertical specimens were manufactured parallel to the build direction (Z direction); the horizontal specimens were manufactured along the transverse to the build direction (XY plane); and 45° specimens were manufactured at an angle of 45° to the build direction. As-built and post-thermally treated blanks were then machined to perform tensile testing according to ASTM E8/E8M − 16. Impact absorbed energy was measured using Charpy impact testing on the as-built and post-thermally treated Charpy blanks according to ASTM E23-18.

3. Results

3.1. Density

Fig. 1 shows a compilation of light micrographs for the as-built condition and post-thermally treated conditions. Results show that the density for the as-built condition (98.6%) remains unchanged after the 980 (98.58%) and SHT thermal treatments (98.63%). During HIP, however, where pressure is also applied simultaneously with heat, part density increases significantly and reaches 99.87%, which can be considered fully dense. The average error calculated for these measurements was found to be 0.1% based on 100 micrographs for each condition (50 in the XY and 50 in the Z direction). The difference in density measured between the directions was less than this calculated error. Post-thermal treatment on its own without external pressure does not affect the shape of porosity as seen from the images in Fig. 1. A mixture of lack-of-fusion (irregular) and gas pores (circular) can be seen to remain in the material after treatments that only involve temperature. After applying pressure along with the temperature during the HIPping process the lack-of-fusion pores have collapsed while the gas porosity was largely unaffected. This is expected as the gas in pores is confined and hence remains in the cavity.

The density results obtained by light microscopy are confirmed using the Archimedes method, as shown in Table 2 below. These results confirm the light micrograph results, where the as-built and only heat treated conditions show similar density. The HIP condition density is significantly higher at 8220 kg/m^3 which is almost the same as that of the wrought material.

Table 1
Heat treatment details.

Name	Treatment details
980	980 °C for 1 h, fast cool to ambient followed by aging
SHT	1200 °C for 1 h, fast cool to ambient followed by aging
HIP	1200 °C for 1 h at 100 MPa argon, fast cool to ambient followed by aging
Aging	720 °C for 8 h, furnace cool over 2 h to 620 °C, hold for 8 h, furnace cool to ambient

3.2. Microstructure

Fig. 2 shows a compilation of a high magnification SEM micrographs from the Z direction (a,c,e) and XY direction (b,d,f) of etched specimens after the 980 (a,b), SHT (c,d) and HIP (e,f) post-thermal treatments.

Fig. 2 (a) shows a SEM micrograph of the 980 sample the Z direction, highlighting the grain boundary and intra-granular white features. The microstructure is characterised by high directionality and possesses needle-like delta phase (δ) [14,15]. Grain boundary needles are about 500 nm thick and have a length of about 2 μm on an average. Intra-granular needles are smaller than the grain boundary needles, with a few 100's of nm in thickness and up to 1 μm in length. The microstructure looks identical to the as-built condition, with Laves phase around the δ needles, reported in Ref. [13].

Fig. 2 (b) shows the 980 sample in the XY direction, demonstrating the grain boundaries and intra-granular features. Needles in size are very similar to the Z direction for the 980 post-thermal condition where grain boundary δ needles are about 500 nm in thickness and between 1 and 3 μm in length on an average. Like the 980 Z direction surface, intra-granular needles are smaller than the grain boundary needles, with a few 100's of nm in thickness and up to 1 μm in length, along with presence of Laves.

Fig. 2 (c) shows several grain boundaries along with details of the features on the etched surface of the Z direction in the SHT post-thermal treated condition. No Laves or δ is seen in the microstructure. However, large white features can be seen at the grain boundaries with a length of about 2 μm and a thickness of about 1 μm. White features can be seen within the grains as well but are smaller with the average diameter being less than 1 μm. The white features are arranged in a discrete pattern along the Z direction, which could be an artefact of their precipitation during the building process. The largest is 1 μm in length and 600 nm in width. Other features are about 500 nm in size. Smaller white features, of a few nanometres in size can be seen interspersed inside the grains without any discernible pattern.

Fig. 2 (d) shows the etched surface in the XY direction, after the SHT post-thermal treatment. Melt pool artefacts and Laves phase have been removed and grain growth is evident compared to 980 treatment [Fig. 1 (b)]. Several white features can be seen at the grain boundaries and within the grains. Black 'tick'-like marks are seen close to the grain boundaries, showing different orientations. Unlike the Z direction, large white features are a lot less common and do not seem to follow any sort of pattern.

Fig. 2 (e) shows the etched Z direction surface of the material after the HIP post-thermal treatment. Microstructure is similar to the SHT condition [Fig. 2 (c)]. The image shows that grain growth has taken place and all melt pool artefacts and Laves phase have been completely

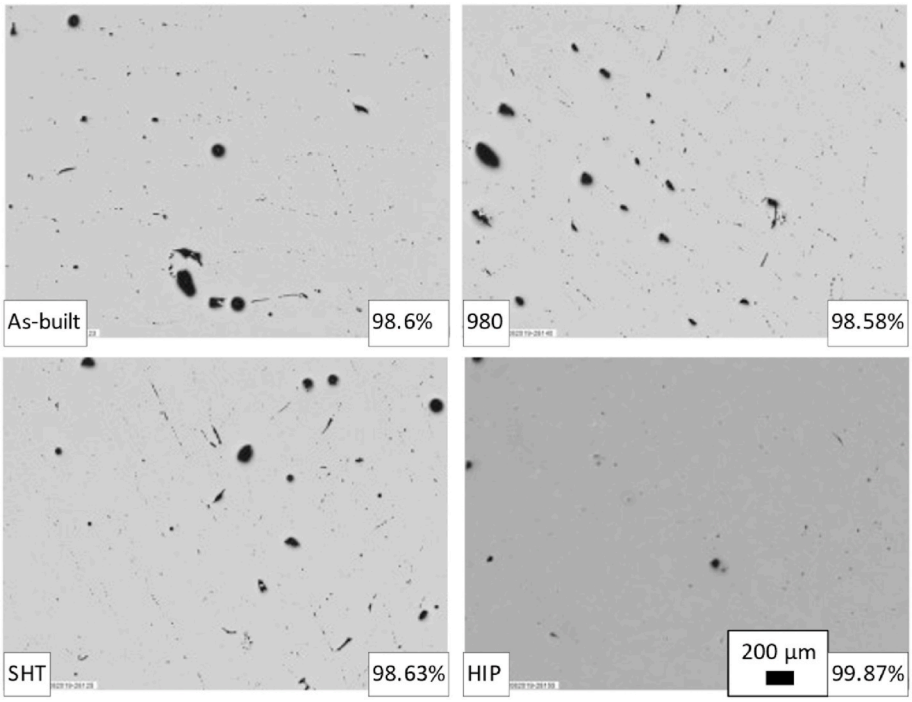

Fig. 1. Compilation of light micrographs and densities for the as-built and various post-thermal treated conditions in the XY direction. The micrographs are representative of the density calculated.

Table 2
Calculated density by Archimedes method.

Specimen	Calculated Density (%)	Calculated Density (kg/m^3)
As-built	98.8 ± 0.18	8125 ± 15
980	98.9 ± 0.15	8131 ± 13
SHT	99 ± 0.19	8134 ± 16
HIP	100 ± 0.09	8220 ± 8

eradicated. Several white features can be seen mainly dispersed within grains. These features seem to be situated on lines, possibly from prior grain boundaries that have been consumed during grain growth. They are sub-micron in width and about 1 µm in length. The presence of white features inside the grains and at the grain boundaries can be seen. Grain boundaries are generally well defined.

Fig. 2 (f) shows the etched XY surface after the HIP post-thermal treatment. Like the Z direction micrograph [Fig. 2 (e)], significant grain growth over the as-built condition is observed along with elimination of any prior melt pool artefacts and Laves phase. In addition, grain boundaries are generally well defined. White features as well as

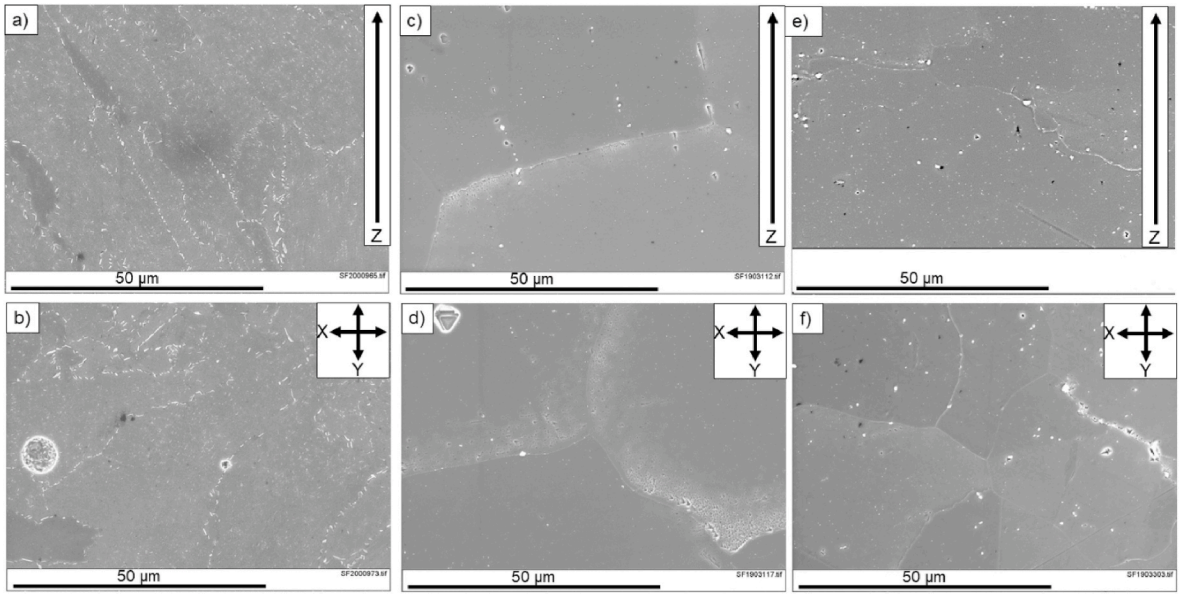

Fig. 2. Compilation of SEM micrographs for the 980 (a,b), SHT (c,d) and HIP (e,f) post-thermal treated conditions. Images a), c) and e) are of the Z direction and b), d) and f) are of the XY direction.

triangular features can be seen at and around the grain boundary on the right side of the image. White features are less in number and dispersed randomly, in contrast to the equivalent image of the Z direction.

3.3. Crystallography and morphology

Fig. 3 shows the EBSD map of the crystal microstructure in the Z (a) and XY (b) directions after the 980 heat treatment. In the first instance the crystal microstructure is identical to that of the as-built condition reported in the previous work [13]. EBSD maps show a substantial difference in structure between the two directions (Z & XY). Z direction map (a) shows that a majority of the grains are columnar in shape running parallel to the build direction and vary in length between 100 and 200 μm. However, these columnar grains are not stacked together, one next to another but are separated by areas where either the grains are at a roughly 45° angle to the build direction, or equiaxed small grains exist. XY direction map (b) shows a distinct microstructure compared to the Z direction. The majority of the grains are irregular and small to medium in size (5–40 μm in diameter). Occasional very large (70–100 μm in length) grains that are roughly circular in shape can be observed. Therefore, it is possible to state that the microstructure at the XY plane is roughly equiaxed in nature. In terms of crystal orientation, inverse pole figure (IPF) colouring reveals that there is no preferred crystallographic direction, as also evidenced by the pole figure for the Z and XY directions.

Fig. 4 shows the EBSD maps after the SHT heat treatment. The crystal microstructure is completely changed over the 980 condition (Fig. 3) with obvious grain growth having taken place. The microstructures of the Z and XY directions are comparable with a mixture of very large grains (>250 μm in length) and very small (<20 μm) grains. In addition, some twinning can be observed in the microstructure in both the Z and XY directions. Qualitatively the disparity between the microstructures has decreased between the two directions. A roughly equiaxed microstructure has developed after the treatment at 1200 °C. In terms of the crystal grain orientation, no persistent coloration suggests that no orientation is preferred over another. The pole figure inserts also show no specific alignment along either the Z direction or the XY direction.

Fig. 5 shows the EBSD maps after HIP. Similar to the SHT condition obvious sign of grain growth can also be seen over the 980 and as-built conditions. Large grains (>250 μm) are mixed with medium size grains (50–100 μm) and smaller grains (10–25 μm) in the Z direction. The XY direction shows a similarly sized grains with the largest grains being smaller than those of the Z direction. The number of twins significantly increases in both the directions over those seen in the SHT condition. For the XY EBSD map, alignment along the [001] direction can be seen in the pole figure. That crystallographic direction is preferred by about 3.26 times than the baseline.

Fig. 6 shows statistical results for the EBSD maps depicted in Figs. 3–5. The grain growth taking place after thermal treatment at 1200 °C is obvious with both the SHT and HIP treatments leading to significantly larger fraction of very big grains in both the Z and XY directions, as can be seen in Fig. 6. While both of the directions in the SHT condition follow a similar pattern in grain size area with localised peaks at around 6000 μm^2, the HIP condition seems to indicate a difference between the directions. However, the scatter of the measured data makes any deduction difficult to quantify, along with the caveat that a single EBSD map were acquired for each condition and direction.

Table 3 show twin analysis results for the EBSD maps presented. In terms of twins, both the SHT and HIP conditions have a comparable number of twinned grains (Table 3). Twins are evenly distributed

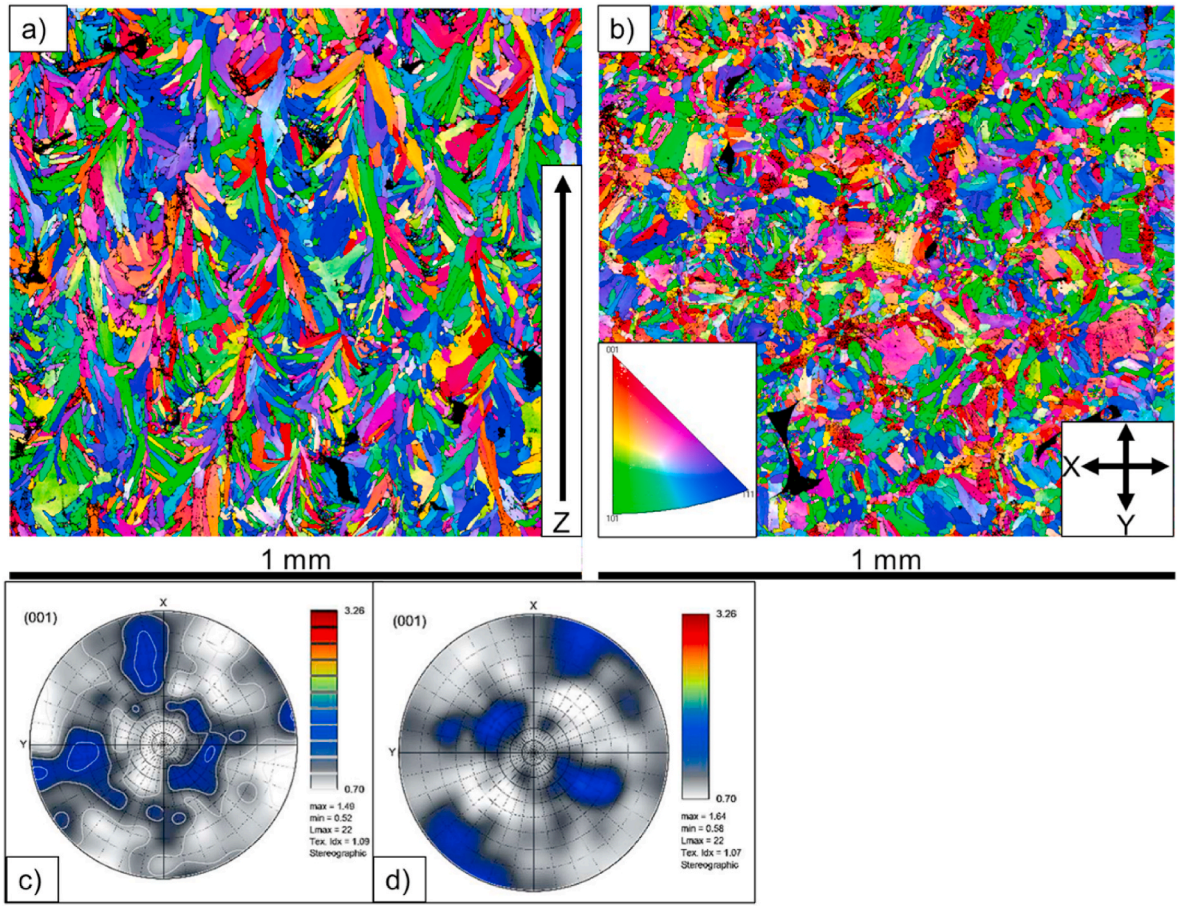

Fig. 3. EBSD maps of the 980 condition showing the Z (a) and XY (b) directions, with the pole figures for the Z (c) and XY directions (d).

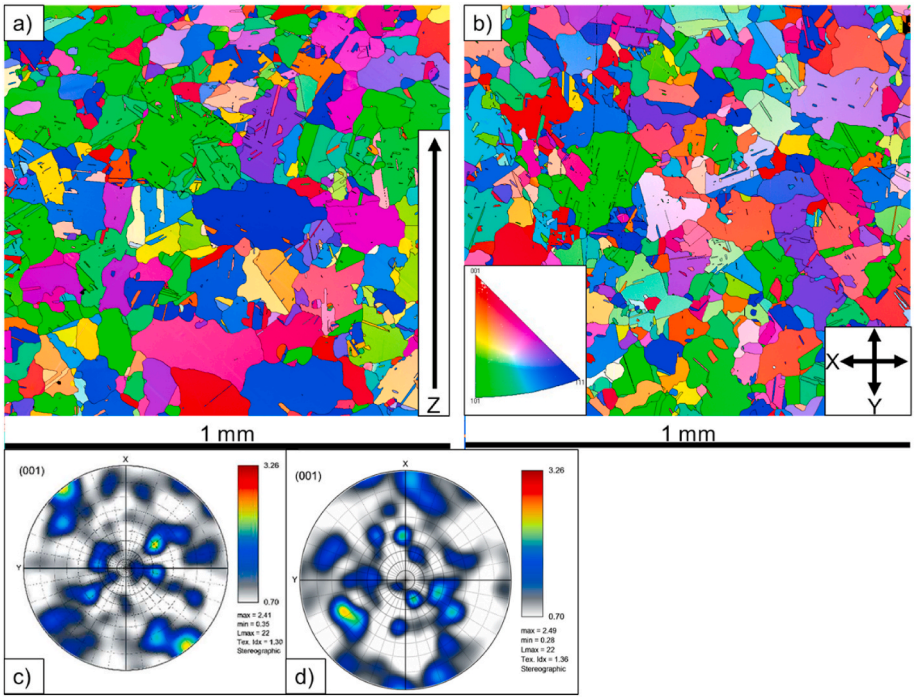

Fig. 4. EBSD maps of the SHT condition showing the Z (a) and XY (b) directions, with the pole figures for the Z (c) and XY directions (d).

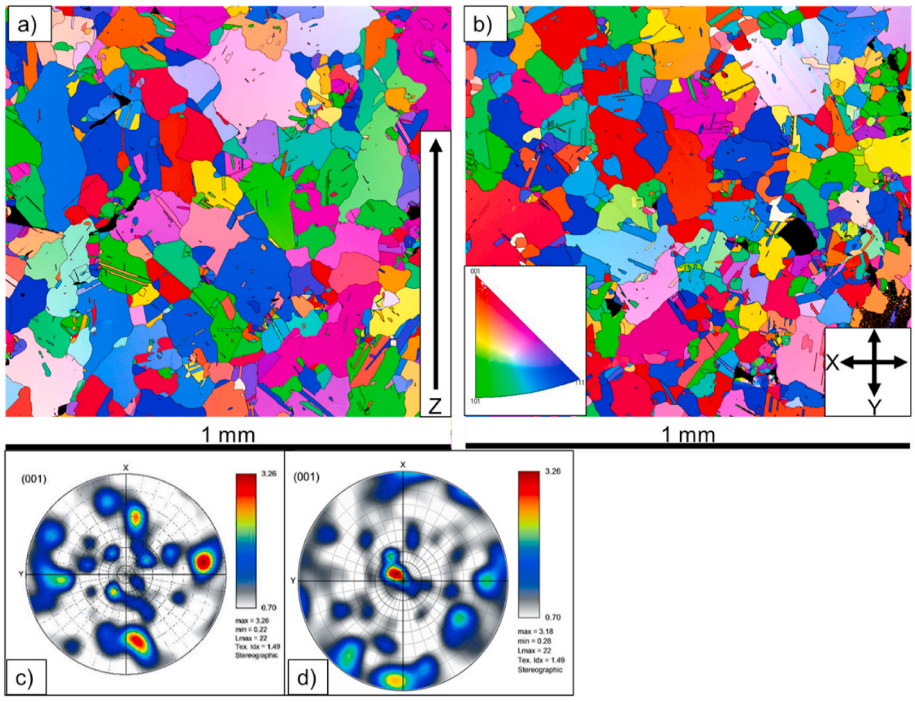

Fig. 5. EBSD maps of the HIP condition showing the Z (a) and XY (b) directions, with the pole figures for the Z (c) and XY directions (d).

between the directions in the HIP condition while the Z direction of the SHT condition has a larger number of twins over total grains (21.72%) than those in its XY direction (12.26%). As the surface fraction of the SHT Z (18.41%) and the SHT XY (18.88%) directions are very similar, it follows that the average size of twinned grains in the XY direction is larger than that in the Z direction. Hence an anisotropy effect to some extend persists in the twinned grain size. Despite the anisotropic result in the SHT condition, the same is not found in the HIP condition where both the percent of twinned grains and the twin areal fraction are very similar between the directions, and larger than that in the SHT condition.

3.4. Tensile properties

Table 4 shows the elevated temperature tensile properties obtained from the as-built and three different post-thermally treated conditions. The as-built condition has an average yield stress (YS) of 726 MPa, ultimate tensile strength (UTS) of 957 MPa and elongation of 19.4%.

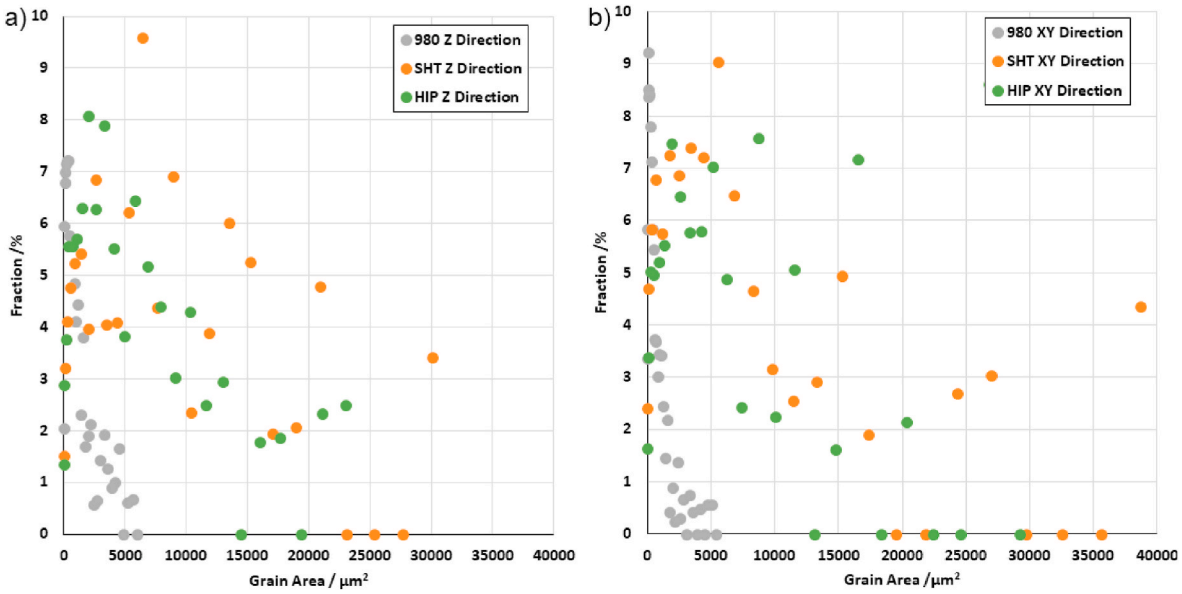

Fig. 6. Fraction of grains versus grain area/size for the Z direction (a) and the XY direction (b), for different post-thermally treated conditions.

Table 3
Number of twins detected in the SHT and HIP EBSD maps (Figs. 4 and 5) with % of grains and % of the surface.

Name	# of twins	% of grains with twins	Surface fraction %
SHT Z	862	21.72	18.41
SHT XY	989	12.26	18.88
HIP Z	1009	33.39	21.34
HIP XY	897	28.93	19.41

Table 4
Elevated temperature (650 °C) tensile properties for alloy 718 L-PBF material in different conditions and orientations along with current aerospace standard requirements.

	Orientation	0.2% YS (MPa)	UTS (MPa)	Elongation (%)
As-built	Vertical	696 ± 11.5	942 ± 7.2	22.8 ± 0.6
	Horizontal	745 ± 6.3	960 ± 5	15.7 ± 0.3
	45° angle	736 ± 4.2	969 ± 3.2	19.7 ± 1.6
980 + Aging	Vertical	1028 ± 11.1	1134 ± 9.4	3.7 ± 0.4
	Horizontal	1087 ± 6.5	1238 ± 1.4	8.2 ± 0.3
	45° angle	1067 ± 0.47	1179 ± 16	4 ± 1.1
SHT + Aging	Vertical	829 ± 6.7	967 ± 1.7	12.1 ± 1.3
	Horizontal	902 ± 6.9	1046 ± 30	10.5 ± 2.3
	45° angle	896 ± 8.8	1009 ± 31	8.5 ± 1.4
HIP + Aging	Vertical	876 ± 6	1023 ± 7.8	13.9 ± 1.3
	Horizontal	956 ± 19	1101 ± 16	13.8 ± 1
	45° angle	862 ± 14	1023 ± 11.7	17.5 ± 1.7
Wrought[a]	N/A	862	1000	12
Cast[b]	N/A	517	576	13.7

[a] From AMS 5662 N [16], elevated temperature minimum requirements.
[b] From AMS 5383F [17], elevated temperature minimum requirements.

These values only satisfy the minimum requirements of the AMS 5383F, aerospace standard for cast alloy 718 material at elevated temperatures. As expected, the 980 condition experiences considerably high levels of strength with an average YS of 1061 MPa, UTS of 1184 MPa and elongation of 5.3%, showing significantly compromised ductility. While the YS and UTS of the 980 condition satisfy the minimum requirements of the AMS 5662N standard (elevated temperature requirements for wrought material), the elongation is significantly distant from the standard requirement. The SHT condition exhibits a mean YS of 876 MPa, UTS 1007 MPa and elongation of 10.4% which comes very close to satisfying the wrought material requirements, with the various orientations satisfying the different requirements. Finally, the HIP condition has an average YS of 898 MPa, UTS of 1049 MPa and elongation of 15.1%. Only the 45° angle specimens are at the limit of not satisfying the minimum YS requirement of the AMS 5662N standard. The HIP material also is on the precipice of satisfying the minimum elongation requirements posed by the AMS 5383F standard.

The results measured at the elevated temperatures are also plotted in Fig. 7 above. The minimum requirements of the AMS standards are plotted as a solid line for the wrought material (AMS 5662N) and a dashed line for the cast material (AMS 5383F).

Fig. 8 shows representative stress-strain curves measured at elevated temperature (650 °C) in all the three post-thermal conditions along with the as-built condition. Note that we did not include all the stress-strain curves obtained in this study to save space.

3.5. Fracture & hardness

Table 5 shows the results of the Charpy impact testing for the as-built, SHT and HIP conditions, for the 980 condition specimen the test failed. Charpy testing shows the amount of absorbed energy a material exhibits at a high-strain rate event and is an indication of ductility versus brittleness. The more energy a material absorbs the more ductile it is. The as-built material absorbed an average of 19.6 J of energy. The SHT material absorbed 26.1 J and the HIP material 47.5 J. In all cases the vertically build specimen absorbed more energy than the horizontal specimen.

Fig. 9 shows the hardness of the material in different conditions (980, SHT & HIP), both aged and unaged at room temperature. The as-built condition has a hardness of 296 HV which drops after post-thermal treatment as expected to 195 and 200 HV for the SHT and HIP conditions respectively. After aging, the material experiences a significant increase in hardness to 463 and 452 HV for SHT and HIP respectively. This reaffirms the fact that the aging treatment has successfully led to the complete precipitation of the strengthening phases (γ' & γ'') [14,18]. The 980 condition was found to have high hardness of 432 and 451 HV regardless of the aging condition, as expected due to the precipitation of a large amount of delta phase.

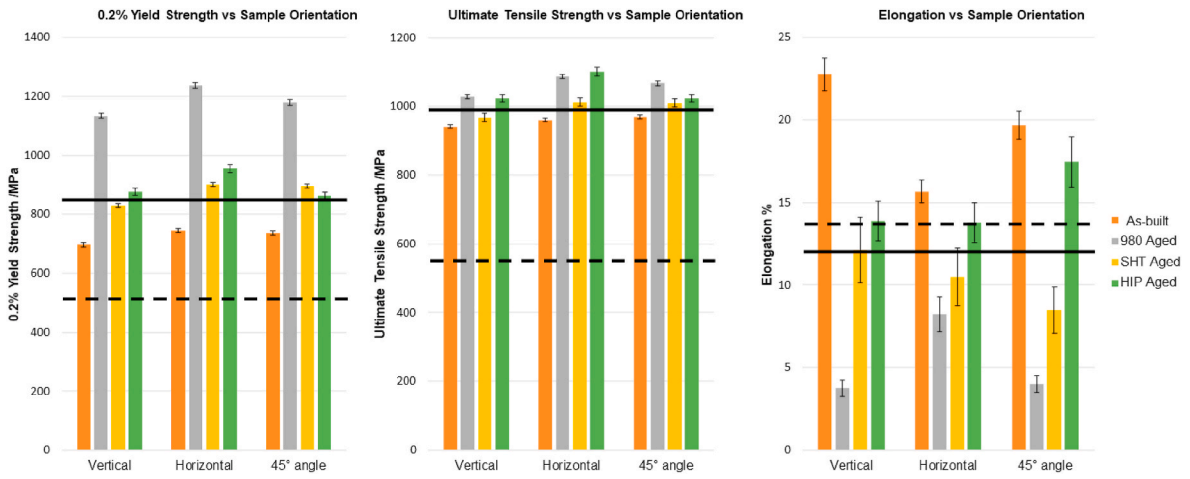

Fig. 7. Elevated temperature (650 °C) tensile test results for different post-thermal treated conditions and specimen orientations with AMS 5662 N (continuous line) and AMS 5383F (dashed line).

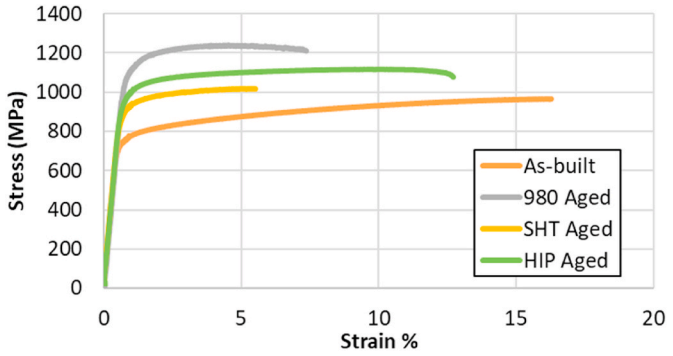

Fig. 8. Illustrative stress–strain curves of the horizontal specimens in different post-thermal treated conditions.

Table 5
Charpy impact test results for different post-thermal conditions of alloy 718 material.

Condition	Orientation	Absorbed Energy/J	Lateral Expansion/mm	Percentage Shear/%
As-built	Vertical	21.9 ± 1.8	0.338 ± 0.073	10
	Horizontal	17.2 ± 0.8	0.161 ± 0.052	10
SHT + Aging	Vertical	32.5 ± 1.1	0.381 ± 0.041	10
	Horizontal	19.6 ± 2.5	0.195 ± 0.012	10
HIP + Aging	Vertical	58 ± 2.7	0.821 ± 0.084	10
	Horizontal	37 ± 2.2	0.542 ± 0.032	23.3

4. Discussion

4.1. Microstructure & porosity

It is well established that alloy 718 microstructure can be modified using post-thermal treatments to control the phase composition of the material. However, the heat treatment techniques used for this purpose have been developed on material produced through the traditional manufacturing methods. Hence, research gaps exist on the effect of post-thermal treatments on material produced through L-PBF.

A major gap concerns the Laves phase, which precipitates during fast cooling of alloy 718 from the molten state to below 1180 °C [14,18]. Prior to AM techniques this problem arose in uncontrolled cooling of cast material, where the Laves phase precipitates preferentially along grain boundaries of the solidifying material [19]. As demonstrated

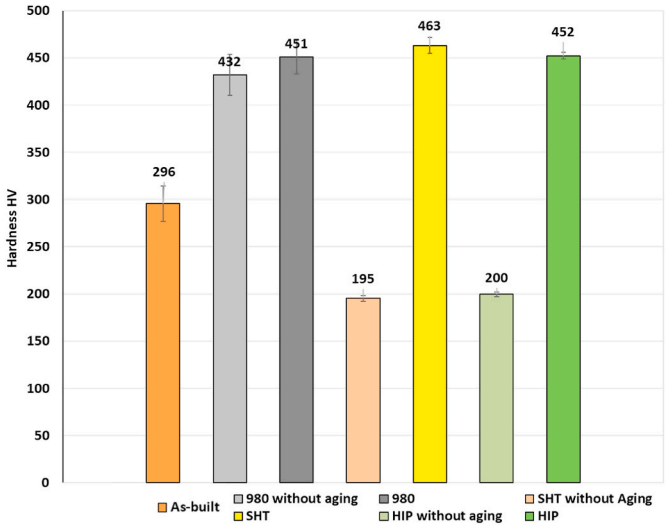

Fig. 9. Hardness values for different conditions of the alloy 718 material.

before [13,20], L-PBF material shows fine distribution of the Laves phase within the microstructure as well as at the grain boundaries due to the continuous rapid cooling as laser scans each layer of the powder bed. The current material standards, developed for cast alloy 718, recommend that heat treatment at 1060 °C will remove the Laves phase [17]. However, the literature shows that even HT up to 1100 °C cannot consistently remove the Laves phase from L-PBF material [8].

The 980 post-thermal treatment performed during the current work shows the problem from following the current heat treatment practices and standards for treating AM material. The temperature used (980 °C) is within the range of the δ phase precipitation, which is between 850 °C and just below 1000 °C [21]. At the same time, Laves is a metastable phase rich in niobium [14,18,19] which combines with the presence of the phase in grains and on grain boundaries, and creates localised areas rich in niobium. The niobium rich locations allow for easy δ phase formation, which is comprised of Nickel and Niobium ($Ni_30{\cdot}8Nb,0.2Ti$). Hence, the Laves phase easily changes to the hard and brittle δ phase. This change is evidenced by the presence of needle-like structures in Fig. 2 (a) & (b), which is the same type of structures seen in literature [7,11,22–25].

Previous studies have shown that the Laves phase in L-PBF alloy 718 material dissolves as temperature gets close to the dissolution temperature (1180 °C) [6–10,12]. The current work has demonstrated that

performing thermal treatment on the material above 1180 °C guarantees the removal of the Laves phase and leaves the microstructure free of any undesired phases. Incipient melting has been reported during high temperature heat treatment of cast material due to melting of the Laves dendrites [26]. However, Laves dendrites in cast material are a few 10's of microns in width versus a few 100's of nanometres in PBF material. This difference in size permits the quick diffusion of Niobium and hence no incipient melting was found in the material treated in the current work.

4.2. Crystal microstructure

In terms of crystal microstructure, the 980 condition shows that no change has taken place from the modulated L-PBF as-built condition reported elsewhere [13] in terms of grain size and orientation. That is to say, the grain shape is partially aligned to the Z direction, with several grains running parallel to it, while in the XY direction significant equiaxed grains exists. The heat treatment also does not affect the orientation of the grains with random distribution and no preferred crystallographic direction observed in the 980 and SHT conditions. The lack of a preferred orientation, in the 980 and SHT conditions, is comparable to results reported in the literature for heat treatments at 980 °C performed on continuous L-PBF alloy 718 material [7,22,24,25,27–29]. Some grain direction preference can be seen in the HIP condition along the [001] direction for the XY EBSD map. The reason for this preference can be traced back to the grain growth.

Literature suggests that grain growth during post-thermal processing can begin at 1040–1060 °C for L-PBF alloy 718 [30]. The extent of crystal grain growth depends on both the temperature and time of the treatment. In prior work, increasing either parameter (temperature or time) led to more extensive grain growth [24,28] but the microstructure remained aligned to the Z direction for material manufactured through continuous L-PBF [24,28,30]. However, in this work, increased grain structure homogeneity between the Z and XY directions is observed after grain growth due to the SHT and HIP treatments which were performed at significantly higher temperatures (1200 °C). The increased homogeneity in microstructure between the two directions (Z & XY) can possibly be traced back to the as-built condition, where for both the directions, the grains show no crystallographic direction preference [13], as demonstrated in the 980 condition in this work. Hence, when grain growth takes place, the growing grains develop along the random directions of the previous microstructure produced during solidification. Since the growth follows random directions, the microstructure stops being aligned to the Z direction and anisotropy seemingly decreases.

Twins have been observed in both the SHT and HIP conditions but not in the 980 condition. Hence, this suggests that twin formation is due to the recrystallization and grain growth that occurs at such high heat treatment temperatures (1200 °C). This has been previously demonstrated for the Z direction [31] as a result of the grain growth occurring at different rates in various areas of the crystal. Twin boundaries would be expected to increase the strength of the material in both the conditions present.

4.3. Mechanical properties

Following the various post-thermal treatments, the specimens built in the horizontal direction still exhibit higher YS and UTS. This is clearly expected for the 980 treatment due to the lack of change in crystal microstructure in comparison with the as-built counterpart, in which the tensile loading is applied normal to the build direction and therefore more grain boundaries result in exhibiting the stronger tensile properties than that of the vertical samples. Any change in the values between 980 & as-built is due to phase differences (γ', γ'' & δ) and similar effects have been widely reported in the literature [7,11,24,32]. However, regarding the SHT and HIP treatments there is no readily apparent reason for the persistence of horizontal orientation having better properties although the crystal microstructure no longer exhibits the unique blend of equiaxed and semi-columnar structure that is normally seen in the as-built condition and the two directions now have a more homogeneous crystal microstructure.

Density can be partially responsible for the difference in measured mechanical properties between SHT and HIP conditions. The main difference between the two conditions is the increase in density from 98.63% in the SHT to 99.87% in the HIP conditions. The measured YS and UTS in the HIP condition are more than 50 MPa higher than those in the SHT condition on average, while elongation also improves by about 2% points on average. Although the differences in the tensile mechanical properties may be attributed to the impact of densification, the differences between directions within the same condition cannot be readily attributed to the density as the different directions have almost the same density. Other factors related to the microstructure such as grain boundary differences and quantity of twins could be the reason for the differences of the directional tensile results, and would be of interest in a specific study of the relationship between microstructure and mechanical properties.

The anisotropic mechanical properties continue in the Charpy results as well, with the outcomes consistently demonstrating that the vertical specimens are more ductile (higher absorbed energy) than the horizontal specimens (lower absorbed energy). Similar to the tensile results, the reason behind the difference between the directions is not readily apparent, considering that the crystal microstructures are very similar. Of interest is that the Charpy results show that the horizontal specimens in the HIP condition were more ductile than the vertical specimens of the SHT condition. This phenomenon might be attributed the presence of porosity. During brittle failure the propagating crack can connect porosity together, decreasing the energy necessary for fracture to occur [33]. Hence, in the denser HIP condition, the microstructure has a chance to absorb more energy and makes the material more ductile.

Along with the material density/porosity change during post-thermal treatment, another effect that may contribute to difference in mechanical properties, is the density of dislocations present in the crystal microstructure. Characterisation of the dislocation density was out of the scope of the current study. However, increased dislocation density has been shown to improve creep performance for L-PBF alloy 718 material [34]. Similarly, dislocation density has been shown to have an impact on the fracture properties of HIP and cast material [35,36]. This phenomenon might explain the mismatch between the measured elongation, which suggests increased ductility, and the Charpy results which suggest increased brittleness for the SHT condition.

Comparing the L-PBF results to current AMS standards it is demonstrated that three conditions (980, SHT & HIP) satisfy the YS and UTS requirements set out for cast material (AMS 5383F). The 980 and HIP conditions also have YS and UTS as high as the wrought standard (AMS 5662N), with the SHT condition being within measurement error distance to hit the requirement. Elongation results, however, are not as easily satisfied. The HIP condition satisfies the wrought material's requirement but is within the measurement error envelope for the cast material. The SHT and 980 conditions fail to satisfy any of the elongation criteria, with only the vertical SHT specimens being close to the wrought material criterion. Hence, the HIP process parameters presented in the current work with possible slight adjustments is capable to produce material that satisfies current aerospace standard requirements for high temperature (650 °C) service.

5. Conclusions

The current work on the post-thermal treatment of alloy 718 material produced through the power modulated L-PBF process has led to the following conclusions:

- Heat treating to a temperature of 980 °C for 1 h led to no change in grain size or orientation. There is evidence of Nb-rich areas around

the finely distributed Laves phase led to the precipitation of needle-like δ phase inside of grains along with the expected δ at grain boundaries.

- A temperature of 1200 °C whether alone (SHT) or with pressure applied (HIP) leads to significant grain growth from the 980 condition to the SHT and HIP conditions, as seen in the grain size analysis of the EBSD data.
- Formation of twinned grains is evident with 1 in 3 grains having a twin in the HIP condition and 1 in 6 grains in SHT condition. No twins were detected in the 980 condition.
- Only material subjected to the HIP process satisfies current elevated temperature aerospace standard requirements for wrought alloy 718. Material subjected to the SHT heat treatment is close to the requirements with further developmental work required.

Declaration of competing interest

The authors declare that they have no known competing financial interests or personal relationships that could have appeared to influence the work reported in this paper.

Data availability

The authors are unable or have chosen not to specify which data has been used.

Acknowledgements

This publication was made possible by the sponsorship and support of Lloyd's Register Foundation. The work was enabled through, and undertaken at, the National Structural Integrity Research Centre (NSIRC), a postgraduate engineering facility for industry-led research into structural integrity established and managed by TWI through a network of both national and international Universities. Lloyd's Register Foundation helps to protect life and property by supporting engineering-related education, public engagement, and the application of research.

References

[1] P.M. Mignanelli, N.G. Jones, M.C. Hardy, H.J. Stone, On the time-temperature-transformation behavior of a new dual-superlattice nickel-based superalloy, Metall. Mater. Trans. A 49 (3) (Mar. 2018) 699–707.
[2] K. Georgilas, Multiscale Experimental and Computational Techniques for Optimising Selective Laser Melting Additive Manufacturing Process Parameters, University of Aberdeen, 2021.
[3] V.P. Kumar, A.V. Jebaraj, Influence of double aging heat treatment on phase transformation and dimensional accuracy of inconel 718 alloy made through laser-based additive manufacturing, Trans. Indian Inst. Met. 74 (12) (Dec. 2021) 3103–3117.
[4] R. M, S. Koppoju, G. Telasang, R. Korla, P. G, Effect of solutionizing temperature on the microstructural evolution during double aging of powder bed fusion-additive manufactured IN718 alloy, Mater. Char. 172 (Feb. 2021), 110868.
[5] S. Raghavan, B. Zhang, P. Wang, C.N. Sun, M.L.S. Nai, T. Li, J. Wei, Effect of different heat treatments on the microstructure and mechanical properties in selective laser melted INCONEL 718 alloy, Mater. Manuf. Process. 32 (14) (2017) 1588–1595.
[6] M.D. Sangid, T.A. Book, D. Naragani, J. Rotella, P. Ravi, A. Finch, P. Kenesei, J. S. Park, H. Sharma, J. Almer, X. Xiao, Role of heat treatment and build orientation in the microstructure sensitive deformation characteristics of IN718 produced via SLM additive manufacturing, Addit. Manuf. 22 (April) (2018) 479–496.
[7] X. Li, J.J. Shi, G.H. Cao, A.M. Russell, Z.J. Zhou, C.P. Li, G.F. Chen, Improved plasticity of Inconel 718 superalloy fabricated by selective laser melting through a novel heat treatment process, Mater. Des. 180 (2019).
[8] W. Huang, J. Yang, H. Yang, G. Jing, Z. Wang, X. Zeng, Heat treatment of Inconel 718 produced by selective laser melting: microstructure and mechanical properties, Mater. Sci. Eng., A 750 (2019) 98–107.
[9] D.J. Newell, R.P. O'Hara, G.R. Cobb, A.N. Palazotto, M.M. Kirka, L.W. Burggraf, J. A. Hess, Mitigation of scan strategy effects and material anisotropy through supersolvus annealing in LPBF IN718, Mater. Sci. Eng., A 764 (July) (2019), 138230.
[10] M.E. Aydinöz, F. Brenne, M. Schaper, C. Schaak, W. Tillmann, J. Nellesen, T. Niendorf, On the microstructural and mechanical properties of post-treated additively manufactured Inconel 718 superalloy under quasi-static and cyclic loading, Mater. Sci. Eng., A 669 (2016) 246–258.
[11] V.A. Popovich, E. V Borisov, A.A. Popovich, V.S. Sufiiarov, D. V Masaylo, L. Alzina, Impact of heat treatment on mechanical behaviour of Inconel 718 processed with tailored microstructure by selective laser melting, Mater. Des. 131 (2017) 12–22.
[12] A. Mostafa, I.P. Rubio, V. Brailovski, M. Jahazi, M. Medraj, Structure, texture and phases in 3D printed IN718 alloy subjected to homogenization and HIP treatments, Metals 7 (6) (2017).
[13] K. Georgilas, R.H.U. Khan, M.E. Kartal, The influence of pulsed laser powder bed fusion process parameters on Inconel 718 material properties, Mater. Sci. Eng., A 769 (Jan. 2020), 138527.
[14] M.J. Donachie, S.J. Donachie, Superalloys: A Technical Guide, second ed., ASM International, Materials Park, OH, 2002.
[15] Y. Desvallees, M. Bouzidi, F. Bois, N. Beaude, Delta phase in INCONEL 718: mechanical properties and forging process requirements, in: E.A. Loria (Ed.), Superalloys 718, 625 and Various Derivatives, 1994, pp. 281–291.
[16] SAE International, AMS 5663N - Nickel Alloy, Corrosion and Heat-Resistant, Bars, Forgings, and Rings 52.5Ni - 19Cr - 3.0Mo - 5.1Cb (Nb) - 0.90Ti - 0.50Al - 18Fe Consumable Electrode or Vacuum Induction Melted 1775 °F (968 °C) Solution and Precipitation Heat Treated, Aerospace Material Specification, 2016.
[17] SAE International, AMS 5383F -Nickel Alloy, Corrosion and Heat-Resistant, Investment Castings 52.5Ni - 19Cr - 3.0Mo - 5.1Cb(Nb) - 0.90Ti - 0.60Al - 18Fe Vacuum Melted Homogenization and Solution Heat Treated, 2018.
[18] R.C. (Roger C. Reed, The Superalloys : Fundamentals and Applications, Cambridge University Press, Cambridge, 2006.
[19] J.F. Radavich, The physical metallurgy of cast and wrought alloy 718, in: Superalloys 718 Metallurgy and Applications (1989), 1989, pp. 229–240.
[20] M.S. Duval-Chaneac, N. Gao, R.H.U. Khan, M. Giles, K. Georgilas, X. Zhao, P.A. S. Reed, Fatigue crack growth in IN718/316L multi-materials layered structures fabricated by laser powder bed fusion, Int. J. Fatig. 152 (Nov. 2021), 106454.
[21] A. Oradei-Basile and J. F. Radavich, "A Current T-T-T Diagram for Wrought Alloy 718." .
[22] S. Azadian, L.-Y. Wei, F. Niklasson, and R. Warren, "PRECIPITATION IN SPRAY-FORMED IN 718." .
[23] D. Zhang, W. Niu, X. Cao, Z. Liu, Effect of standard heat treatment on the microstructure and mechanical properties of selective laser melting manufactured Inconel 718 superalloy, Mater. Sci. Eng., A 644 (2015) 32–40.
[24] M. Ni, S. Liu, C. Chen, R. Li, X. Zhang, K. Zhou, Effect of heat treatment on the microstructural evolution of a precipitation-hardened superalloy produced by selective laser melting, Mater. Sci. Eng., A 748 (December 2018) (Mar. 2019) 275–285.
[25] Y. Gao, D. Zhang, M. Cao, R. Chen, Z. Feng, R. Poprawe, J.H. Schleifenbaum, S. Ziegler, Effect of δ phase on high temperature mechanical performances of Inconel 718 fabricated with SLM process, Mater. Sci. Eng., A 767 (Nov. 2019), 138327.
[26] T. Antonsson and H. Fredriksson, "The Effect of Cooling Rate on the Solidification of INCONEL 718." .
[27] V.A. Popovich, E. V Borisov, A.A. Popovich, V.S. Sufiiarov, D. V Masaylo, L. Alzina, Functionally graded Inconel 718 processed by additive manufacturing: crystallographic texture, anisotropy of microstructure and mechanical properties, Mater. Des. 114 (2017) 441–449.
[28] J. Strößner, M. Terock, U. Glatzel, Mechanical and microstructural investigation of nickel-based superalloy IN718 manufactured by selective laser melting (SLM), Adv. Eng. Mater. 17 (8) (2015) 1099–1105.
[29] D. Zhang, W. Niu, X. Cao, Z. Liu, Effect of standard heat treatment on the microstructure and mechanical properties of selective laser melting manufactured Inconel 718 superalloy, Mater. Sci. Eng., A 644 (Sep. 2015) 32–40.
[30] E. Chlebus, K. Gruber, B. Kuźnicka, J. Kurzac, T. Kurzynowski, Effect of heat treatment on the microstructure and mechanical properties of Inconel 718 processed by selective laser melting, Mater. Sci. Eng., A 639 (2015) 647–655.
[31] Y. Cao, P. Bai, F. Liu, X. Hou, Y. Guo, Effect of the solution temperature on the precipitates and grain evolution of IN718 fabricated by laser additive manufacturing, Materials 13 (2) (Jan. 2020) 340.
[32] Z. Wang, K. Guan, M. Gao, X. Li, X. Chen, X. Zeng, The microstructure and mechanical properties of deposited-IN718 by selective laser melting, J. Alloys Compd. 513 (2012) 518–523.
[33] P. Bidare, A. Jiménez, H. Hassanin, K. Essa, Porosity, cracks, and mechanical properties of additively manufactured tooling alloys: a review, Adv. Manuf. 10 (2) (Jun. 2022) 175–204.
[34] J.J. Shi, X. Li, Z.X. Zhang, G.H. Cao, A.M. Russell, Z.J. Zhou, C.P. Li, G.F. Chen, Study on the microstructure and creep behavior of Inconel 718 superalloy fabricated by selective laser melting, Mater. Sci. Eng., A 765 (Sep. 2019), 138282.
[35] Z. Oksiuta, N. Baluc, Microstructure and Charpy impact properties of 12–14Cr oxide dispersion-strengthened ferritic steels, J. Nucl. Mater. 374 (1–2) (Feb. 2008) 178–184.
[36] O.M. Horst, B. Ruttert, D. Bürger, L. Heep, H. Wang, A. Dlouhý, W. Theisen, G. Eggeler, On the rejuvenation of crept Ni-Base single crystal superalloys (SX) by hot isostatic pressing (HIP), Mater. Sci. Eng., A 758 (Jun. 2019) 202–214.